Direct Measurement of the Spin-Orbit Interaction in a Two-Electron InAs Nanowire Quantum Dot

C. Fasth,[1] A. Fuhrer,[1,*] L. Samuelson,[1] Vitaly N. Golovach,[2] and Daniel Loss[2]

[1]*Solid State Physics/Nanometer Consortium, Lund University, P.O. Box 118 Lund, Sweden*

[2]*Department of Physics and Astronomy, University of Basel, Klingenbergstrasse 82, CH-4056 Basel, Switzerland*

(Received 8 January 2007; published 26 June 2007)

We demonstrate control of the electron number down to the last electron in tunable few-electron quantum dots defined in catalytically grown InAs nanowires. Using low temperature transport spectroscopy in the Coulomb blockade regime, we propose a method to directly determine the magnitude of the spin-orbit interaction in a two-electron artificial atom with strong spin-orbit coupling. Because of a large effective g factor $|g^*| = 8 \pm 1$, the transition from a singlet S to a triplet T^+ ground state with increasing magnetic field is dominated by the Zeeman energy rather than by orbital effects. We find that the spin-orbit coupling mixes the T^+ and S states and thus induces an avoided crossing with magnitude $\Delta_{SO} = 0.25 \pm 0.05$ meV. This allows us to calculate the spin-orbit length $\lambda_{SO} \approx 127$ nm in such systems using a simple model.

DOI: 10.1103/PhysRevLett.98.266801 PACS numbers: 73.23.Hk, 71.70.Ej, 73.63.Kv

Semiconducting nanowires are presently subject to an intense research effort due to their potential as nanoscale building blocks for components such as p-n junctions [1], field effect transistors [2], logical elements [3], and single electron circuits [4]. For spintronic or quantum electronic applications, e.g., qubits and quantum gates [5], accurate control over the electron number down to the last one as well as precise control over the spin state [6] and the coupling between spins in neighboring quantum dots [7] are required. Furthermore, the spin-orbit interaction is of crucial importance since coupling of the spin to orbital degrees of freedom, and thus charge determines spin relaxation and decoherence rates, which in turn determines decay rates for spin qubits. It is thus of fundamental interest to experimentally determine the spin-orbit length λ_{SO} as accurately as possible. The spin-orbit interaction is, on the other hand, also a pathway to directly manipulate the spin state of a quantum dot electrically rather than with conventional electron spin resonance techniques. In this context, it was recently suggested to employ the spin-orbit coupling for all electrical spin manipulation [8], an approach which has the potential to be considerably faster than other schemes. Here we discuss few-electron quantum dot formation in homogeneous InAs nanowires, where the confined region is achieved by electrical depletion through local gate electrodes. This technique allows for highly tunable quantum dot systems with strong spin-orbit coupling where size, coupling, and electron number starting from zero are easily controlled by external voltages, and the spin-orbit length λ_{SO} can be determined from a simple measurement of the anticrossing between singlet and triplet states.

InAs nanowires were grown using chemical beam epitaxy with 40 nm Au catalyst particles, yielding untapered nanowires with a diameter of $\sim$50 nm. For details on growth, see Ref. [9]. Electronic transport experiments show these wires to be n-type and have a mean free path $\ell \approx 100$ nm [10]. For the fabrication of gate-induced quantum dots, the wires are deposited onto a grid of gold electrodes, which is covered by a thin SiN dielectric layer. Using this technique, we have previously demonstrated formation of gate-defined single and double many-electron quantum dots [11]. Here, due to refined sample fabrication involving thinner nanowires, more densely spaced electrodes (periodicity 60 nm), and a thinner SiN layer (18 nm), the control over the potential landscape in the nanowire has been greatly improved, allowing tunability down to the last electron.

The wire and five gate electrodes are contacted individually with Ni/Au contacts [12] [see Fig. 1(a) and the inset in Fig. 1(b)]. The bias is applied symmetrically across the wire [11,13], and measurements were performed in a dilution refrigerator at an electron temperature $T_e = 80$ mK. We apply negative voltages to gates 1 and 4 to locally deplete the electron density in the wire and form potential barriers, inducing a quantum dot above gates 2 and 3. Figure 1(b) shows Coulomb blockade diamonds measured with gates 2 and 3 used as plunger gates. In the following, we refer to the plunger gate voltage as $V_G = V_{g3}$ and emphasize here that V_{g2} is always tuned simultaneously as in Fig. 1(b). Inside each diamond, the electron number N on the dot is fixed, while at each diamond apex close to zero bias the dot ground state energies for N and $N + 1$ electrons are degenerate and transport can occur. In Fig. 1(b), no further degeneracy points are observed for $V_G < -0.94$ V, and the diamond border lines continue without kinks, indicating that the quantum dot is empty [14]. The diamond border line conductance peaks correspond to the quantum dot chemical potential being aligned to μ_D or μ_S, as indicated in Fig. 1(b). Additional peaks in the differential conductance represent transitions involving excited states.

In addition to conductance peaks originating in dot states, Fig. 1(b) also shows an abundance of weak and densely spaced peaks, which are related to the low-

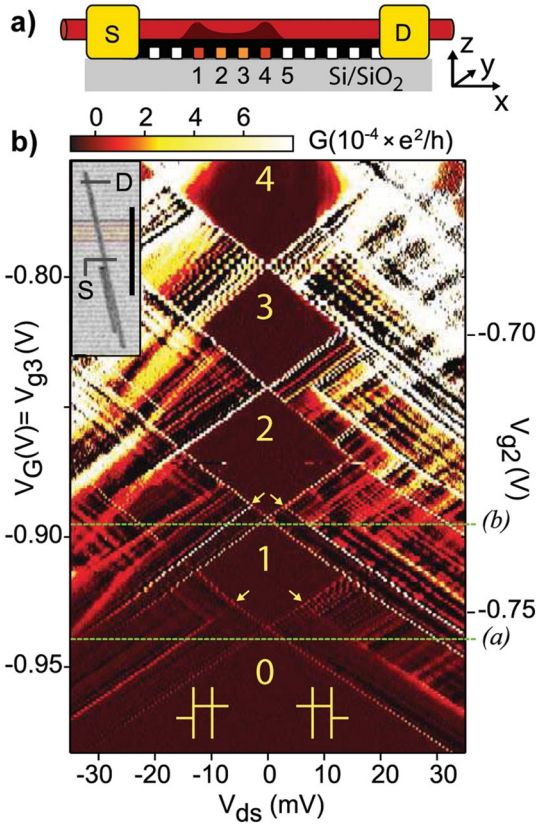

FIG. 1 (color). (a) Sample schematic showing the Au grid covered in SiN (black) and the nanowire (red) on top. The source and drain contacts and the five individually contacted gates are indicated. (b) Differential conductance measured as a function of $V_{\rm ds}$ and plunger gate voltages. The other gates are set to $V_{g1} = -2.56$ V, $V_{g4} = -1.65$ V, and $V_{g5} = 2.5$ V, respectively. Electron numbers are indicated in yellow, and the inset shows a scanning electron microscopy image of the wire on the electrode grid, with a 1 μm scale bar.

dimensional nature of the source and drain leads [14]. The unused local gates beneath the wire are set to +2.2 V in order to tune the leads towards metallic behavior and avoid accidental dot formation. However, the relatively short mean free path and a coherence length which at $T = 100$ mK extends over the full nanowire, together with the radial confinement, cause a varying density of states in the leads which leads to these resonances. This is also consistent with the observation of negative differential conductance lines.

To separate these lead effects from the quantum dot states, we apply a magnetic field B perpendicular to the substrate plane and measure the differential conductance along two cuts in Fig. 1(b) detecting the ground and excited state lines of the quantum dot with one (a) and two (b) electrons. For the one-electron case, the peaks in Fig. 2(a) on either side of the zero bias split with increasing B, reflecting transport through the Zeeman-split first ($\uparrow, \downarrow$) and second ($\Uparrow, \Downarrow$) orbital levels. In low-dimensional systems, the electronic g factor g^* depends on system size and dimensionality. It is often found to be strongly reduced from the bulk modulus, which for InAs is $|g^*| \approx 14.7$ [15,16]. From the Zeeman splitting of orbitals 1 and 2, we extract the effective g factors $|g_1^*| = 8 \pm 0.4$ and $|g_2^*| = 8.9 \pm 1$. As expected, these values are smaller than the bulk modulus but consistent with previous experiments performed on similar nanowires [14,16].

In Fig. 2(b), we identify the two-electron ground state peak (◆) as the transition from a singlet S to spin-up which involves tunneling of a $\downarrow$ electron and therefore moves to higher energy with increasing B. For the three triplet excited states T^+, T^0, and T^-, we find two lines (□/■) involving transitions $T^+ \rightarrow \uparrow$ and $T^0 \rightarrow \downarrow$ (□) or transitions $T^0 \rightarrow \uparrow$ and $T^- \rightarrow \downarrow$ (■). Here the first two transitions (□) require tunneling of a $\uparrow$ electron, and the transition line moves to lower energy with increasing B, while in the other two cases (■) a $\downarrow$ electron tunnels, and the line shows a slope similar to that of the ground state line. In the following, we refer to the two excited state lines as μ_{T^0} and μ_{T^+}, corresponding to the two dot states carrying most of the current [17]. The splitting $\mu_{T^0} - \mu_{T^+}$ allows us to extract $|g_T^*| = 8 \pm 0.5$ similar to the one-electron values. In quantum dots defined in GaAs heterostructures, this splitting is typically observed only when a large B is applied in-plane with the two-dimensional electron gas since the g factor in these systems is much smaller and orbital effects dominate for perpendicular fields.

A quantitative analysis of our data takes into account asymmetries in the capacitive coupling from source and drain to the quantum dot. The conductance peak slopes in Fig. 1(b) change with bias and plunger gate voltage and differ between states. This indicates that the relation between V_G, $V_{\rm ds}$ and the energy levels of the quantum dot is nonlinear. We therefore allow the gate lever arm $\alpha_G = C_G/C_\Sigma$ to depend on V_G but not on $V_{\rm ds}$ and the source-drain coupling asymmetry $\delta\alpha = \alpha_S - \alpha_D$ to vary with $V_{\rm ds}$, where $\alpha_{S(D)} = C_{S(D)}/C_\Sigma$ is the source (drain) lever arm [13]. C_Σ is the self-capacitance of the dot, and $C_{G,S,D}$

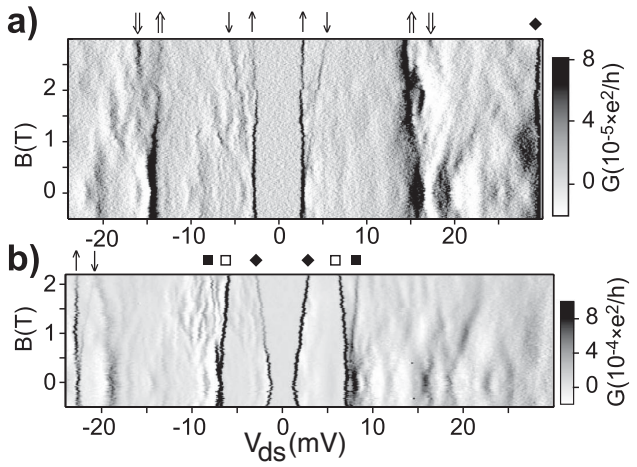

FIG. 2. Evolution of the differential conductance peaks as a function of B along the two cuts (a) and (b) in Fig. 1(b).

denote the respective relative capacitive couplings. From the two diamond border slopes at each degeneracy point ($V_{ds} \approx 0$), we extract α_G's which can be approximated as $\alpha_G(V_G) = 0.32 - (V_G + 0.905\ \mathrm{V})/2.27\ \mathrm{V}$. For symmetric coupling of the dot to source and drain, it follows $\delta\alpha = 0$. Using $\alpha_G(V_G)$, we rescale Fig. 1(b), eliminating the dependence of border line slopes on V_G. The remaining variations in the slopes are then attributed to a V_{ds}-dependent $\delta\alpha$, which can be determined from these same slopes. For nonzero $\delta\alpha$, the energy shift of the quantum dot levels with V_{ds} relative to source or drain is given by $[1 \mp \delta\alpha(V_{ds})]eV_{ds}/2$, respectively.

The necessity of this correction scheme becomes clear when we extract the single-particle orbital splitting $\Delta\varepsilon = \varepsilon_2 - \varepsilon_1$ from Fig. 1(b) and plot the bare bias splitting for negative (blue dots) and positive (red dots) V_{ds} as a function of V_G in Fig. 3(a). The splittings clearly deviate at most V_G's, but after the correction is applied the splittings for negative (blue squares) and positive (red squares) V_{ds} are nearly identical, and we find $\Delta\varepsilon \approx 6.5$ meV, changing by less than 4% in the measured interval. The magnetic field dependence of $\Delta\varepsilon$ is extracted from Fig. 2(a), and we find a quadratically decreasing behavior [see Fig. 3(b)]. Upon closer inspection, this trend is already visible in the raw data in Fig. 2(a), and similar results were obtained in quantum dots with a 2D harmonic confinement [18,19]. For comparison, we apply a similar harmonic confinement model [14,20] and extract $\hbar\omega_x = 6.3$ meV and $\hbar\omega_y = 40$ meV from the fit indicated by the black line. This is in agreement with the device geometry from which we expect that the dot is elongated along the nanowire. We further estimate an effective size $2\lambda_x = 2\sqrt{\hbar/m^*\omega_x} = 46$ nm and $2\lambda_y = 18$ nm.

For the two-electron case, we determine the singlet-triplet splitting at $B = 0$ with $\Delta_{ST} = \mu_T - \mu_S$ [see Fig. 3(c)]. Again the two bias directions give the same result after the correction has been applied, and Δ_{ST} decreases from 3.2 to 2.8 meV over the measured gate voltage range. The opposite dependence of Δ_{ST} on plunger gate voltage was previously observed in a lateral gate-defined quantum dot in a GaAs-based two-dimensional electron gas and attributed to shape deformation of the parabolic potential [21,22].

For the magnetic field dependence of Δ_{ST} [see Fig. 3(d)], we consider two splittings $\Delta_{ST^+} = \mu_{2,T^+} - \mu_{2,S}$ and $\Delta_{ST^0} = \mu_{2,T^0} - \mu_{2,S}$. Δ_{ST^0} shows only a small shift with B, which we attribute to orbital and interaction effects. Because of the large Zeeman splitting between the triplet states, Δ_{ST^+} shows a strong linear decrease with increasing B. In addition, we have extracted the Coulomb interaction energy $U = 13.5$ meV between two electrons on the first orbital using the corresponding conductance peak splitting in Fig. 1(b). We found U to be independent of V_G and B within the investigated ranges.

The inset in Fig. 4(a) gives the magnetic field dependence of μ_T and μ_S similar to that in Fig. 2(b) but over an extended magnetic field range. At $B \approx 3.8$ T (see white arrow), the quantum dot undergoes a transition where the two-electron ground state changes from S to T^+. This area is enlarged in the main panel, and, in contrast to the usually observed crossing [22,23], the S-T transition in our data

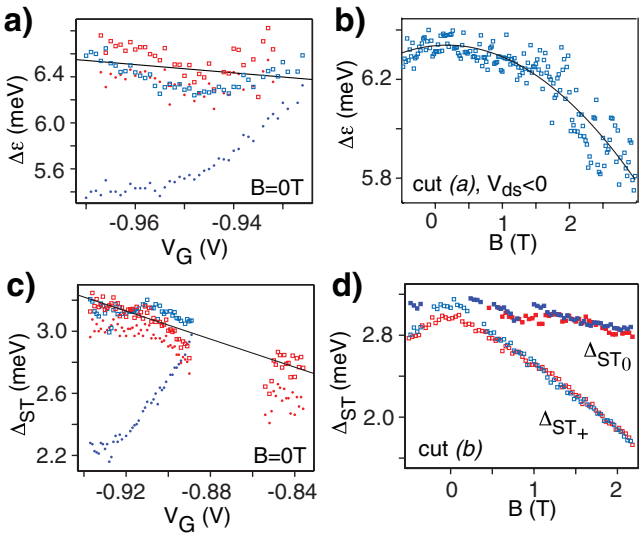

FIG. 3 (color). Orbital splitting $\Delta\varepsilon$ and singlet-triplet splitting Δ_{ST} as a function of V_G and B. In (a) and (b), $\Delta\varepsilon$ was derived from the corrected difference between ↑ and ⇑ [see Figs. 1(b) and 2(a)]. In (c), Δ_{ST} was calculated from the data in Fig. 1(b), and in (d) both splittings Δ_{ST^+} (□) and Δ_{ST^0} (■) were extracted from Fig. 2(b). For comparison, the small dots in (a) and (c) indicate the bare bias splittings for negative (blue) and positive (red) V_{ds}.

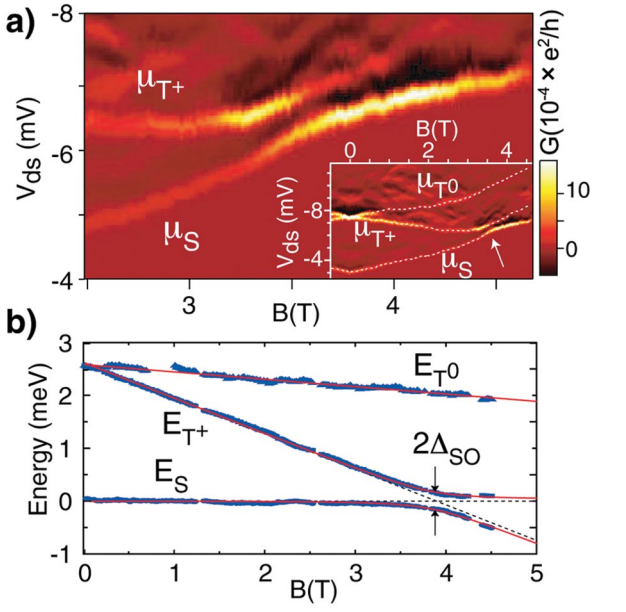

FIG. 4 (color). (a) Inset: Singlet-triplet transition from cut (*b*) in Fig. 1 after gate voltages have been optimized. (a) Main panel: Enlargement of the transition between μ_{T^+} and μ_S exhibiting a clear anticrossing. (b) Energy levels extracted from the corrected peak splittings in (a) together with a fit to a simple model indicated by the red lines.

clearly shows an avoided crossing due to the spin-orbit interaction [24]. We then extract the separation of these three chemical potentials, and, by assuming that the singlet energy E_S is independent of B, we can reconstruct the spectrum of the two-electron artificial atom as shown in Fig. 4(b). The magnitude of the anticrossing is $\Delta_{\mathrm{SO}} = 0.23$ meV and serves as a direct measure of the spin-orbit interaction strength in such quantum dots.

The InAs nanowires are known to have wurtzite crystal structure [16], despite the fact that bulk wurtzite InAs does not exist. The wurtzite crystal has a reduced symmetry compared to zinc-blende structures, and, because of s-p_z mixing, additional spin-orbit terms linear in momentum occur for the conduction band electrons in bulk materials. In nanowires, like in most nanosystems, an important role is played by the boundary and additional spin-orbit terms arise in asymmetric structures, such as ours. Generally, the spin couples to the longitudinal motion of the electron with a spin-orbit interaction that in first order of $\boldsymbol{k} \cdot \boldsymbol{c}$ assumes the following general form:

$$H_{\mathrm{SO}} = (\boldsymbol{k} \cdot \boldsymbol{c})(\boldsymbol{\gamma} \cdot \boldsymbol{\sigma}), \tag{1}$$

where $\boldsymbol{c}$ is a unit vector along the wurtzite hexagonal axis (c axis) and $\boldsymbol{\gamma} = (\gamma_x, \gamma_y, \gamma_z)$ is a vector of coupling constants. In a Hund-Mulliken approximation for the elongated nanowire quantum dot [14], this general form of the spin-orbit interaction leads to efficient mixing of the S and T^+ states with the magnitude of the anticrossing given by

$$\Delta_{\mathrm{SO}}(B) = \frac{E_Z}{\sqrt{2}} \frac{r_{12}\tilde{m}^*_{\|}}{\hbar^2} \sqrt{\gamma_x^2 + \gamma_y^2} = \frac{E_Z}{\sqrt{2}} \frac{r_{12}}{\lambda_{\mathrm{SO}}}, \tag{2}$$

where $E_Z = g^* \mu_B B$ is the Zeeman energy, $r_{12} = \langle \psi_T | (x_1 - x_2) | \psi_S \rangle$ is an effective distance between the two electrons, and $\tilde{m}^*_{\|}$ is the electron effective mass in the nanowire in a magnetic field. The red lines in Fig. 4(b) are a fit to the standard expression for level repulsion

$$E_{1,2} = \frac{E_S + E_{T_+}}{2} \pm \sqrt{\frac{(E_S - E_{T_+})^2}{4} + \Delta_{\mathrm{SO}}^2}, \tag{3}$$

where the bare singlet energy was set to be constant $E_S = 0$ and $E_{T_+} = E_{T_0} - g^* \mu_B B$, with $E_{T_0} = -\gamma_B B$. We assume that r_{12} does not depend on B. This means that Δ_{SO} increases linearly with magnetic field and yields an asymmetric splitting when comparing the left with the right-hand side of the anticrossing. The linear dependence of E_{T_0} on magnetic field is an experimental finding consistent with all acquired data sets and characterized by the phenomenological parameter $\gamma_B = 0.14$ meV/T. At $B \approx 3.8$ T where the bare levels cross (dashed lines), we find $E_Z \approx 1.8$ meV and estimate $r_{12} \approx \lambda_x = 23$ nm, which allows us to calculate the spin-orbit length $\lambda_{\mathrm{SO}} \approx 127$ nm from Eq. (2). Finally, it is interesting to note that, even though we extracted λ_{SO} directly from the level structure of a strongly confined two-electron system, it is comparable in magnitude to $\tilde{\lambda}_{\mathrm{SO}} \approx 200$ nm obtained for unconfined electrons in similar InAs nanowires [10].

This work was supported by the Swedish Foundation for Strategic Research (SSF), the Swedish Research Council (VR), the Swiss NSF, NCCR Nanoscience Basel, and ICORP JST (V. G. and D. L.).

*Electronic address: fuhrer@nigra.ch

[1] K. Haraguchi *et al.*, Appl. Phys. Lett. **60**, 745 (1992); Y. Cui and C. M. Lieber, Science **291**, 851 (2001).
[2] A. B. Greytak *et al.*, Appl. Phys. Lett. **84**, 4176 (2004); J. Goldberger *et al.*, J. Phys. Chem. B **109**, 9 (2005).
[3] Y. Huang *et al.*, Science **294**, 1313 (2001).
[4] C. Thelander *et al.*, Appl. Phys. Lett. **83**, 2052 (2003); S. D. Franceschi *et al.*, Appl. Phys. Lett. **83**, 344 (2003); W. Lu *et al.*, Proc. Natl. Acad. Sci. U.S.A. **102**, 10 046 (2005); Z. Zhong *et al.*, Nano Lett. **5**, 1143 (2005); M. T. Björk *et al.*, Nano Lett. **4**, 1621 (2004); A. Pfund *et al.*, arXiv:cond-mat/0701054.
[5] D. Loss and D. P. DiVincenzo, Phys. Rev. A **57**, 120 (1998); G. Burkard, D. Loss, and D. P. DiVincenzo, Phys. Rev. B **59**, 2070 (1999).
[6] F. H. L. Koppens *et al.*, Nature (London) **442**, 766 (2006).
[7] J. R. Petta *et al.*, Science **309**, 2180 (2005).
[8] V. N. Golovach, M. Borhani, and D. Loss, Phys. Rev. B **74**, 165319 (2006); C. Flindt, A. S. Sorensen, and K. Flensberg, Phys. Rev. Lett. **97**, 240501 (2006); S. Debald and C. Emary, Phys. Rev. Lett. **94**, 226803 (2005).
[9] B. J. Ohlsson *et al.*, Physica (Amsterdam) **13E**, 1126 (2002).
[10] A. E. Hansen *et al.*, Phys. Rev. B **71**, 205328 (2005).
[11] C. Fasth *et al.*, Nano Lett. **5**, 1487 (2005).
[12] D. B. Suyatin *et al.*, Nanotechnology **18**, 105307 (2007).
[13] T. Ihn, *Electronic Quantum Transport in Mesoscopic Semiconductor Structures*, Springer Tracts Mod. Phys. Vol. 192 (Springer, New York, 2004), pp. 78–80.
[14] See EPAPS Document No. E-PRLTAO-98-021723 for supplementary information. For more information on EPAPS, see http://www.aip.org/pubservs/epaps.html.
[15] A. A. Kiselev, E. L. Ivchenko, and U. Rössler, Phys. Rev. B **58**, 16 353 (1998).
[16] M. T. Björk *et al.*, Phys. Rev. B **72**, 201307(R) (2005).
[17] The two processes $T^- \rightarrow \downarrow$ and $T^0 \rightarrow \downarrow$ also contribute to the current but are less probable and found to be suppressed in our experiment. This is likely due to fast spin relaxation combined with weak coupling to the leads. The process $T^- \rightarrow \uparrow$ is forbidden by selection rules.
[18] S. Tarucha *et al.*, Phys. Rev. Lett. **77**, 3613 (1996).
[19] M. Ciorga *et al.*, Phys. Rev. B **61**, R16 315 (2000).
[20] B. Schuh, J. Phys. A **18**, 803 (1985).
[21] J. Kyriakidis *et al.*, Phys. Rev. B **66**, 035320 (2002).
[22] D. M. Zumbühl *et al.*, Phys. Rev. Lett. **93**, 256801 (2004).
[23] L. P. Kouwenhoven, D. G. Austing, and S. Tarucha, Rep. Prog. Phys. **64**, 701 (2001); C. Ellenberger *et al.*, Phys. Rev. Lett. **96**, 126806 (2006).
[24] J. R. Petta and D. C. Ralph, Phys. Rev. Lett. **87**, 266801 (2001).